

Energy loss versus exit angle for H^+ and He^+ ions channeled in Au $\langle 100 \rangle$ at very low energies, and observation of a molecular effect for incident H_2^+

E. A. Figueroa, E. D. Cantero, J. C. Eckardt, G. H. Lantschner, M. L. Martiarena, and N. R. Arista
*División Colisiones Atómicas, Centro Atómico Bariloche and Instituto Balseiro, Comisión Nacional de Energía Atómica,
 8400 San Carlos de Bariloche, Argentina*

(Received 8 July 2008; published 10 September 2008)

The variation of the energy loss versus the exit angle in channeling experiments using H^+ , He^+ , and H^+ fragments produced by the incidence of H_2^+ on thin gold crystals oriented in the $\langle 100 \rangle$ direction has been investigated in the low-velocity range, corresponding to energies below 10 keV/u. The experimental results for H^+ and He^+ were compared with computational simulations performed with the MARLOWE code, considering an impact-parameter-dependent energy loss based on electron density calculations and low-energy stopping power models. The comparisons provide information on the impact-parameter dependence of the energy loss for channeled ions and serve as a test of theoretical models in the present low-energy range. A molecular effect is observed for the transmitted H^+ fragments corresponding to H_2^+ incidence. This effect is explained based on geometrical considerations and a vicinage effect in the energy loss of correlated protons.

DOI: [10.1103/PhysRevA.78.032901](https://doi.org/10.1103/PhysRevA.78.032901)

PACS number(s): 34.50.Bw, 61.85.+p

I. INTRODUCTION

The channeling phenomenon was discovered and formally established by computer simulations and experiments in the early 1960s [1–5], and is today a well-known phenomenon in the area of ion-solid interactions and materials analysis; a general theory to describe the effect was developed by Lindhard in 1965 [6]. A recent review provides a good coverage of the field of research [7].

The energy loss and its angular dependence for light ions in gold and other materials have been studied experimentally and theoretically for monocrystalline and polycrystalline samples [8–20], mostly for intermediate and high energies. The problem of angular effects in the energy loss of channeled ions at low energies is, however, a less explored question. Since the mean density of the valence electrons in an open crystalline channel is lower than the one seen along a random direction, one expects differences in the energy loss of ions in the two cases. This effect has been observed and studied in different crystallographic directions of various elements at high energies [3–5] and also observed in low-energy experiments using thin monocrystalline samples by detecting the ions emerging at 0° with respect to the original beam direction [21,22].

There is both theoretical and experimental interest in quantifying the channeling effect in the energy loss, particularly in the low- to very low-energy range (velocities below the Bohr velocity v_0 , down to $\sim 0.2v_0$), which is a demanding range both for experiments and for a theoretical understanding of the basic interaction processes. A subject of particular interest is the case of channeling of a pair of protons produced simultaneously by the fragmentation of H_2^+ incident on monocrystalline foils. The existence of a so-called vicinage effect in the channeling of correlated protons was predicted long ago [23], but experimental evidence for the low-energy range was obtained only recently [24].

In this work we present measurements of energy losses of slow H^+ , H^+ fragments from H_2^+ , and He^+ ions transmitted through a thin gold monocrystal along the $\langle 100 \rangle$ direction, as

a function of the exit angle in the velocity range below 10 keV. The study includes computer simulations based on the MARLOWE code [25] and comparisons with solid-state electron density calculations and low-energy stopping power models. Finally, a simple model is presented to analyze the vicinage effect in the energy loss observed in experiments using H_2^+ beams.

II. EXPERIMENT

The ion beams were generated in an electrostatic accelerator with a hot discharge ion source followed by a mass selection filter and electrostatic bending for elimination of neutrals (Fig. 1). The emerging ions were energy analyzed by a rotatable electrostatic spectrometer with 1.5% resolution and detected by an electron multiplier followed by pulse-processing electronics and a multichannel scaler. The monocrystalline Au targets oriented in the $\langle 100 \rangle$ direction were mounted perpendicular to the beam direction on a 3 mm transmission-electron-microscope grid. The thicknesses, determined by energy-loss measurements and comparison with previous channeling stopping power experiments [22], were 120 and 134 Å, respectively. With this setup the energy-loss values have been determined with a dispersion of ± 5 eV and an accuracy of $\pm 10\%$, the main error source being the accuracy of the reference stopping power values.

The angle of detection θ was changed by rotating the analyzer around the target in a plane containing the incident

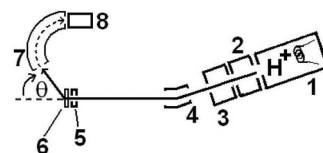


FIG. 1. Schematic experimental setup. (1) Ion source. (2) Acceleration and focusing stages. (3) Wien filter. (4) Electrostatic deflector. (5) Secondary electron collector. (6) Gold sample. (7) Rotatable electrostatic analyzer. (8) Electron multiplier.

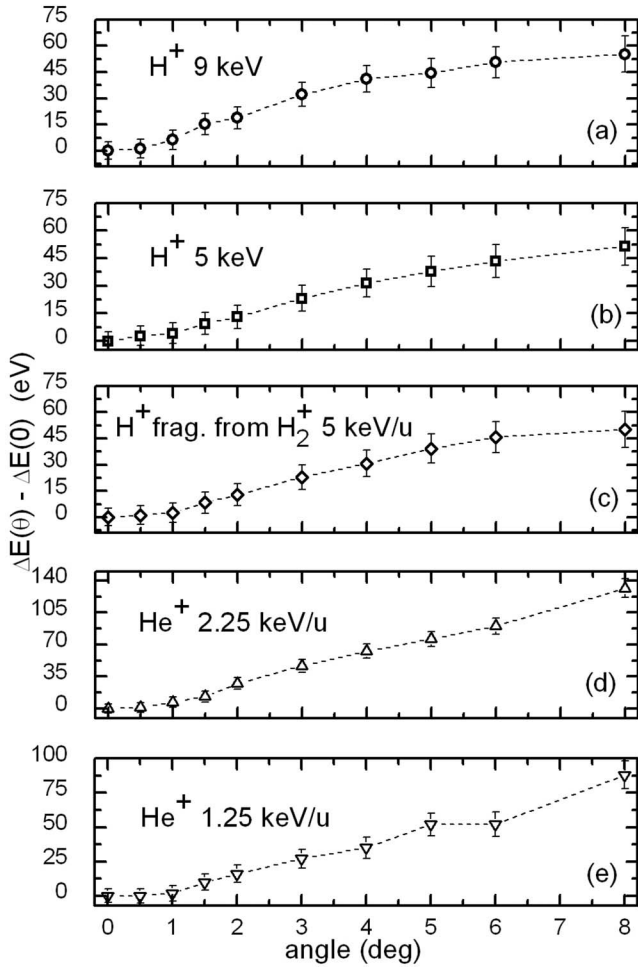


FIG. 2. Experimental values of the energy loss versus detection angle for (top to bottom) (a) 9 keV H⁺, (b) 5 keV H⁺, (c) 5 keV/u H₂⁺ fragments, (d) 2.25 keV/u He⁺, and (e) 1.25 keV/u He⁺. (a) corresponds to a 120 Å foil, and (b)–(e) to a 134 Å foil. The values of the energy loss at zero angle are the following: (a) 1008, (b) 782, (c) 764, (d) 1007, and (e) 695 eV.

beam direction. The acceptance angles of the spectrometer were 0.5° along the detector’s direction of motion, and 1.8° in the perpendicular direction. Further experimental information was given in Ref. [20].

A. Experimental results

In Fig. 2 we show the experimental results obtained for (a) 9 keV H⁺, (b) 5 keV H⁺, (c) 5 keV/u H⁺ fragments from H₂⁺, (d) 2.25 keV/u He⁺, and (e) 1.25 keV/u He⁺ in gold foils of thicknesses 120 [case (a)] and 134 Å [cases (b)–(e)]. The values of ΔE in this figure are the mean values of the energy-loss spectra obtained from two or more measurements, with the corresponding zero-angle values ΔE(0) subtracted (see figure caption). In the restricted angular range considered here, other well-known effects that contribute to the angular dependence, such as path-length enlargement and variation of the nuclear energy loss [19], are of negligible incidence. In the experiments with H₂⁺ the experimental values correspond to the energy losses of the protons emerging

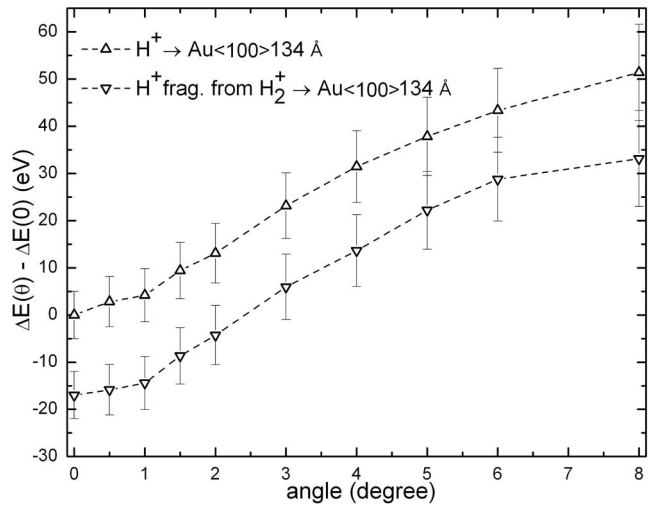


FIG. 3. Variation of the energy loss with emergence angle for 5 keV H⁺ channeled in a 134 Å foil, and for the H⁺ fragments resulting from 5 keV/u H₂⁺, channeled in the same foil. In both cases the energy-loss values have been referred to the value measured for single protons at zero exit angle.

as a result of the dissociation of the molecular ion. It may be noted that the energy losses for channeling conditions are smaller than the corresponding values for random incidence (or in polycrystalline gold foils) by a factor ~0.7–0.9 (this agrees with previous measurements by Blume *et al.* [10,22]).

In Fig. 3 we compare the energy losses of the transmitted protons obtained by the incidence of H⁺ with those of the dissociation fragments of H₂⁺. We observe a nearly constant difference of about 20 eV between both curves. To gain further insight into this effect, we show in Fig. 4 the energy loss spectrum of the emerging H⁺ fragments from H₂⁺ and the corresponding spectrum of H⁺ arising from the incidence of protons with the same velocity. We observe a coincidence of the curves on the side of high energy losses and a significant

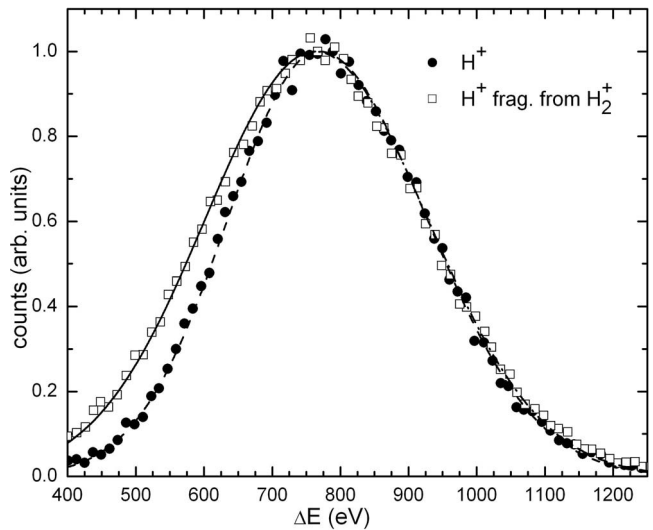


FIG. 4. Experimental spectra for 5 keV H⁺ and for H⁺ fragments from 5 keV/u H₂⁺ transmitted through a 134 Å foil, measured at zero exit angle.

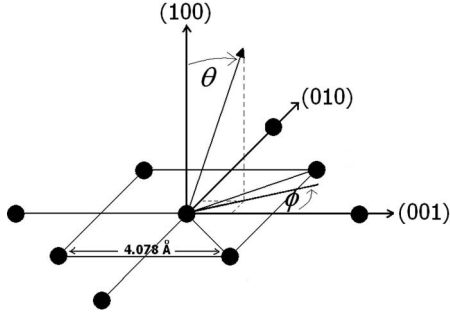


FIG. 5. Coordinate system used in the computer simulations: the family of $\langle 100 \rangle$ planes is perpendicular to the \hat{z} axis. The detection angle θ and azimuthal angle ϕ are also indicated.

difference at the low-energy-loss flank. The figure corresponds to measurements at zero angle but the same behavior was observed at all the measured angles. A model explaining this behavior is presented in a forthcoming section of this paper.

III. COMPUTER SIMULATION

The energy loss simulations were performed using the MARLOWE code [25], which is a standard code for atomic collisions in solids. The fcc gold crystal target was oriented with the $\langle 100 \rangle$ planes perpendicular to the beam direction. The lattice vibrations are taken into account by the Debye model, considering the crystal at room temperature. The coordinate system used in the simulations is shown in Fig. 5, where the \hat{z} axis is oriented toward the inside of the sample and perpendicular to the $\langle 100 \rangle$ planes.

The interaction of the moving ions with the crystal is represented by the Molière potential, namely,

$$V(r) = \frac{Z_1 Z_2}{r} \sum_{i=1,2,3} b_i e^{-r/\gamma_i}, \quad (1)$$

where $\gamma_i = a/\Gamma_i$. The constant a is the screening parameter and was chosen following Lindhard,

$$a = \beta \frac{0.8853 a_0}{(Z_1^{2/3} + Z_2^{2/3})^{1/2}}, \quad (2)$$

here Z_1 and Z_2 are the atomic numbers of projectile and target, a_0 is the Bohr radius, $\Gamma_i = \{0.3, 1.2, 6\}$, and $b_i = \{0.35, 0.55, 0.1\}$. The factor β is a correction coefficient taken from Ref. [26]; for H and He ions interacting with gold it is very close to 1.

The inelastic energy-loss model combines an impact-parameter-independent term with an impact-parameter-dependent one, with a separation coefficient α (a model parameter whose value is in the range 0–1) [25]. The energy transfer to target atoms was simulated using two alternative models. In the first case, we used the Oen-Robinson model [27] for the impact-parameter dependence, given by

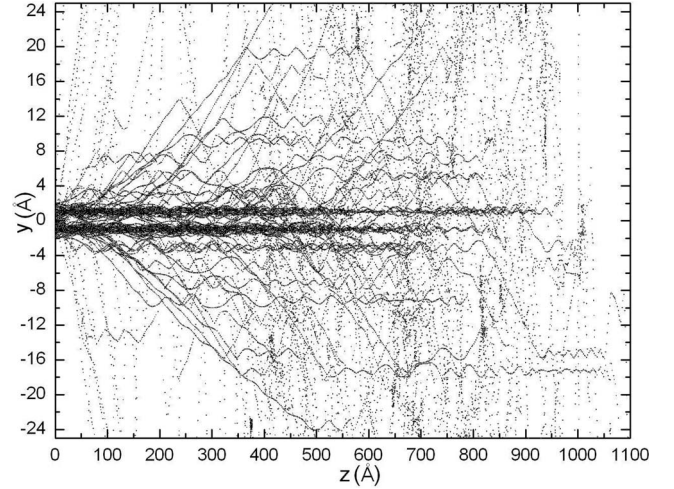


FIG. 6. Ion trajectories for 5 keV protons penetrating a gold sample oriented along the $\langle 100 \rangle$ direction.

$$\Delta E_{\text{OR}}(p) \equiv \alpha \frac{S_e}{\pi r_{\text{max}}^2} + (1 - \alpha) \frac{S_e e^{-p/\gamma_1}}{2\pi \gamma_1^2 \kappa}. \quad (3)$$

The first term of the sum in Eq. (3) represents the nonlocal contribution, where r_{max} is an equivalent atomic radius of the target, while the second term contains the impact-parameter dependence in the original form proposed by Oen and Robinson in terms of the minimum distance of approach p of the ion to a target atom, and with $\kappa = 1 - (1 + r_{\text{max}}/\gamma_1) e^{-r_{\text{max}}/\gamma_1}$.

Second, we propose an alternative model for the impact-parameter dependence in the form of a Gaussian function, given by

$$\Delta E_g(p) \equiv \alpha \frac{S_e}{\pi r_{\text{max}}^2} + (1 - \alpha) \frac{S_e e^{-p^2/\gamma'^2}}{\pi \gamma'^2 \kappa'}, \quad (4)$$

where $\kappa' = 1 - e^{-r_{\text{max}}^2/\gamma'^2}$ and γ' is a parameter that may be fixed by comparison with *ab initio* calculations [28–30] or by adjustment to the experimental data. S_e is the electronic stopping cross section, obtained from the experimental result, by $S_e = (1/N)(\Delta E/\Delta x)$, where ΔE is the energy loss at zero angle, N is the atomic density, and Δx is the thickness of the sample.

For comparison with the experiments, the elliptical angular acceptance geometry of the rotatable electrostatic spectrometer was taken into account in the analysis of the simulation results. For a more complete analysis, the simulated detector plane can be rotated with respect to the initial ion direction or, equivalently, the sample can be rotated by the azimuthal angle ϕ .

A. Results of the simulations

In Figs. 6 and 7 we show two examples of proton trajectories obtained from this simulations, where the characteristics of the channeling phenomenon are very clearly observed. Figure 6 gives a general view of the process and covers a wide range of thickness; it shows trajectories of dechanneling as well as others that indicate rechanneling in parallel

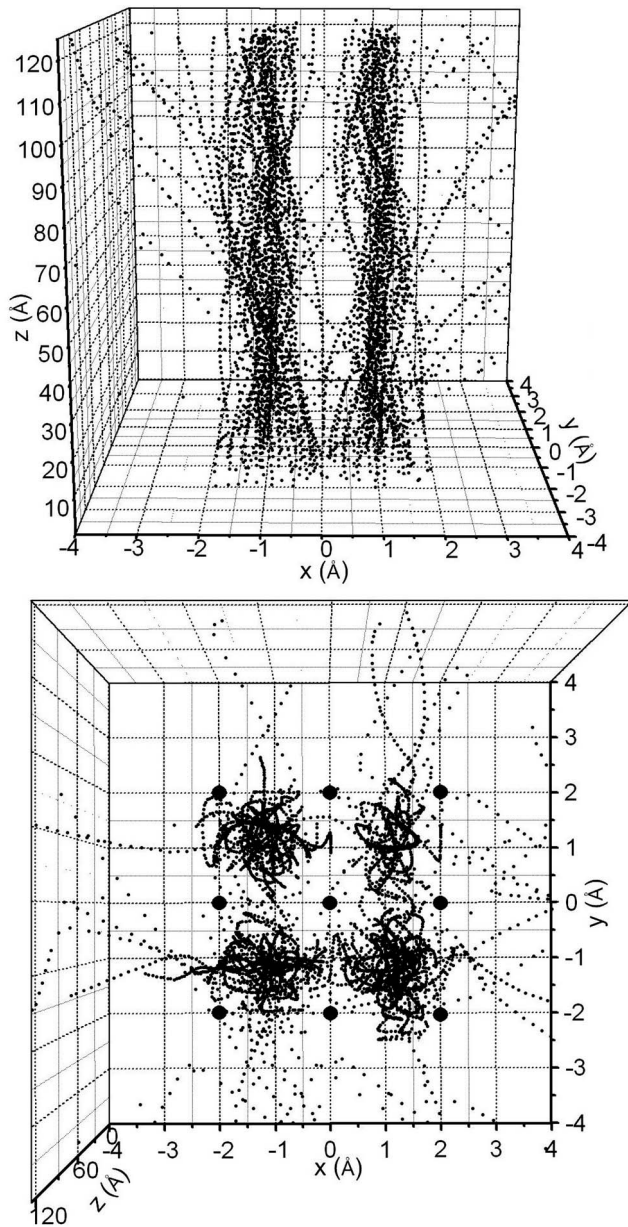


FIG. 7. Ion trajectories for 9 keV protons moving in a gold target along the $\langle 100 \rangle$ channel.

channels. The ends of the trajectories correspond to implantation sites. The nine spots in the lower graph of Fig. 7 show columns of atoms. In this figure the confined character of the trajectories is clearly observed.

Let us consider now the results of these simulations. We show in Fig. 8 the average of simulated energy-loss curves for azimuthal angles varying from 0° to 45° , for (a) 9 and (b) 5 keV H^+ channeled in 120 and 134 Å foils, respectively, compared with the experimental data. The triangles show the average of the Gaussian model, the squares the results of the Oen-Robinson model. To reproduce the experiments in the best way in these cases we used values of $\alpha=0.90$ and 0.85 , respectively. Figure 9 shows experimental and simulation results for (a) 2.25 and (b) 1.25 keV/u He^+ transmitted in the same 134 Å Au $\langle 100 \rangle$ sample. With the exception of one data point in case (b), the comparisons are similarly good as in

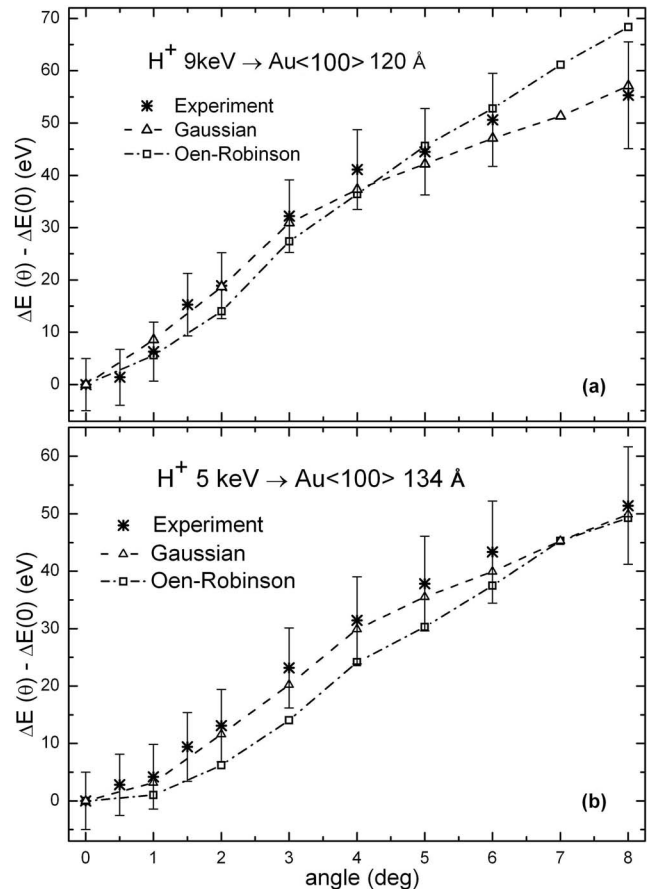


FIG. 8. Angular dependence of the energy loss of 9 and 5 keV protons transmitted through 120 and 134 Å Au $\langle 100 \rangle$ samples. The star symbols show the experimental values, while the symbols joined by lines show the simulation results using the Oen-Robinson and Gaussian models.

the previous cases. For these cases we used values of $\alpha=0.80$ and 0.70 respectively.

In our energy range, the simulation results showed a weak dependence of the energy loss on the impact parameter. The physical reason for this behavior may be attributed to the relatively small inhomogeneity of the electron density distribution within the channels of the gold crystal (at least for the regions explored by low-energy light ions). The best agreement between the simulations and the experiments is obtained when the relative contribution of the impact-parameter-independent term in Eq. (3) is approximately between 70% and 90% (i.e., between $\alpha=0.70$ and 0.90) for all the cases studied.

IV. DISCUSSION AND COMPARISON WITH THEORETICAL CALCULATIONS

The results of a large number of simulations and comparisons with experiments may be cast in a more illustrative way by considering the impact-parameter dependence of the energy transfer from the incident ion to the electrons of a target atom, with the purpose of reaching physical insight into the characteristics of the energy-loss mechanism involved in the

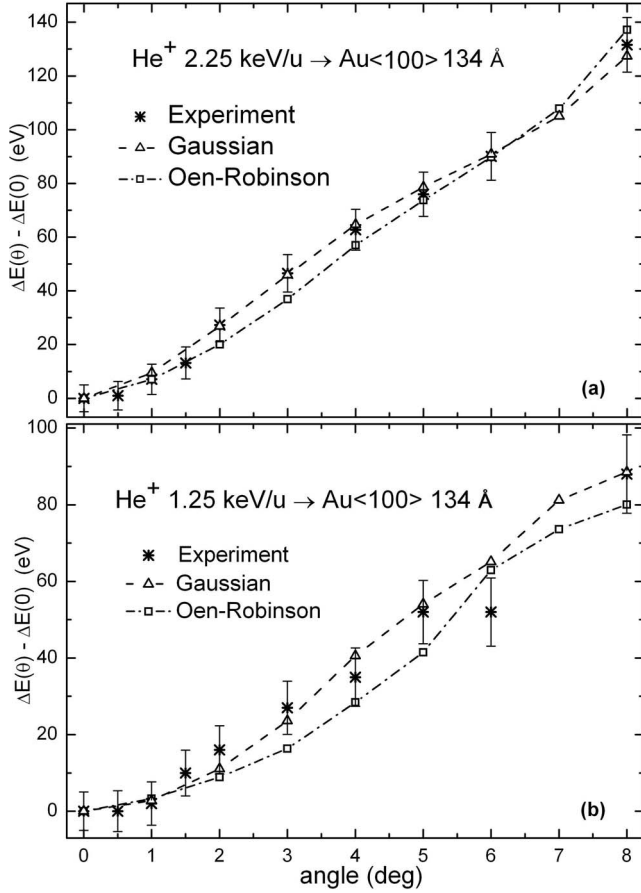


FIG. 9. Angular dependence of the energy loss of 2.25 keV/u He⁺ and 1.25 keV/u He⁺ transmitted through a 134 Å Au <100> sample. The star symbols show the experimental values, while the symbols joined by lines show the simulation results using the Oen-Robinson and Gaussian models.

channeling process, and also to allow comparisons with theoretical models. Figure 10 shows the position dependence of the local stopping force for 5 keV protons channeled in a Au crystal. The line with circles (ZBL-LA) shows the values of the local stopping power calculated according to the transport cross section approach of Lifschitz and Arista (LA) [31] and using the local density approximation (LDA) [32], with the electronic density of gold calculated by Ziegler *et al.* (ZBL) [33], while the line with triangles (VV-LA) is a similar calculation using the electronic density Valdés and Vargas (VV) from Ref. [30] and the stopping model of Ref. [31] (LA). The most frequent value for the impact parameter obtained from this simulation is in the range of the stopping minimum, $r_{mf} \approx 1.44$ Å, which is also the geometrical center of the channel.

To obtain the values of the local stopping power according to the LDA approach, the following procedure was applied: first we determine the local values of the free electron gas parameter r_s as a function of the local density $n(r)$ in the solid [which provides $r_s[r] \equiv r_s(n(r))$]; then the local stopping is calculated as $dE/dx[r] = n(r)v v_F[r] \sigma_{tr}[r]$, where $v_F[r] = 1.919/r_s[r]$ is the local Fermi velocity, and $\sigma_{tr}[r]$ is the transport cross section for slow protons in a free electron gas [31] with Fermi velocity $v_F[r]$. The present treatment is

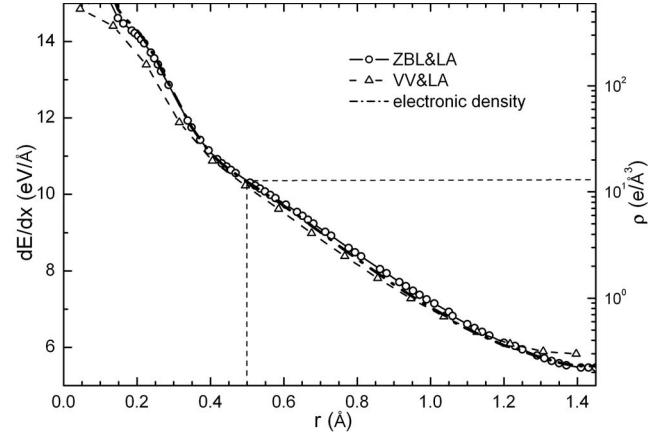


FIG. 10. Radial dependence (with respect to a gold atom) of the calculated local stopping power for 5 keV protons in a Au crystal, according to the LDA, with the stopping model of Ref. [31] (AL), and using *ab initio* calculations of electron densities from Refs. [30] (VV) and [33] (ZBL). The box region delimited with dotted lines indicates the region of impact parameters explored by the present experiments. The dash-dotted line (partially superposed on the previous curves) shows the local electron density using the logarithmic scale on the right-hand side, and matching with the stopping curves at $r=0$ and 1.44.

appropriate to describe the region of ion velocities below the Fermi velocity [32,34,35].

The use of the local density approximation assumes a direct relation of the local stopping power with the electron density; however, it should be noted that, while at high energies this connection is nearly linear [36], at low energies the density dependence is much weaker. This is due to a cancellation effect imposed by the Pauli principle on a Fermi gas [37]. In particular, we find that in most of the pertinent range considered here the dependence is of the form $dE/dx[r] = v\{A \log_{10}[n(r)] + B\}$. To illustrate this, we have included in Fig. 10 a plot of the electron density shown with a logarithmic scale on the right-hand side. Almost perfect coincidence with the energy-loss curves is observed.

In order to compare the theoretical values with those deduced from the computer simulations, we translate the radial dependence of the stopping power to an equivalent impact-parameter dependence of the energy loss. For this purpose, the impact-parameter dependence of the energy transfer to the target electrons $\Delta E(p)$ is obtained by integrating dE/dx over a straight path with impact parameter p as follows:

$$\Delta E_{\text{theor}}^{\text{LDA}}(p) \equiv \frac{\xi}{N\pi r_{\text{max}}^2} + \frac{1}{C} \int \left(\frac{dE}{dx}[r] - \xi \right) dx, \quad (5)$$

where the first term yields the contribution of the impact-parameter-independent term in Eqs. (3) and (4) and ξ is a constant (impact-parameter-independent) stopping force determined at the radial distance r_{max} (where the localized contribution may be neglected). It represents the stopping force corresponding to a uniform electron gas. In the second term, C is a constant used to constrain the total electronic stopping cross section value S_e and is given by

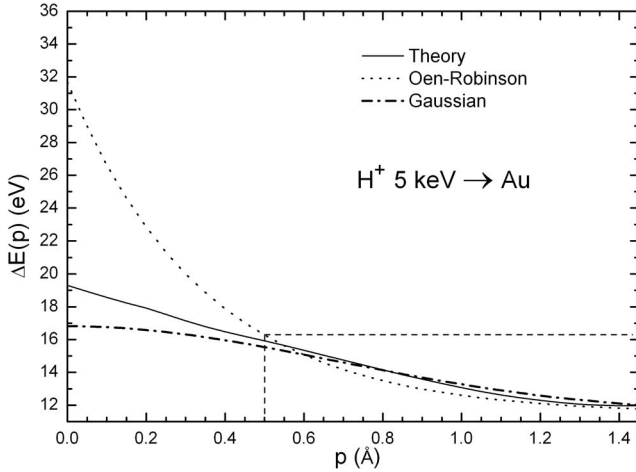


FIG. 11. Impact-parameter dependence of the energy transfer to the target electrons ΔE for 5 keV protons channeled in Au. The figure shows the Oen-Robinson and Gaussian models together with the theoretical calculations using the ZBL and LA approach of Fig. 10. The box region delimited with dotted lines indicates the region of impact parameters explored by the present experiments.

$$C = \frac{\iint \left(\frac{dE}{dx}[r] - \xi \right) 2\pi p \, dx \, dp}{S_e - S_e^{\text{nl}}}, \quad (6)$$

where $S_e^{\text{nl}} = \xi/N$ is the nonlocal stopping cross section contribution. In Eq. (5) we have split the theoretical stopping values into two terms, nonlocal and local contributions, to allow a comparison in similar terms with the values obtained from the simulations. The integration is carried out considering a sphere of radius $r_{\text{max}} = 1.57 \text{ \AA}$, corresponding to the equivalent volume of a Au atom in the solid. In Fig. 11 we show the impact-parameter dependence of the energy transfer ΔE to the target electrons per atom for 5 keV protons channeled in 120 \AA Au foil, obtained by this procedure. The parameter γ' in Eq. (4) was determined by adjusting the Gaussian approximation to the theoretical curve and comparing with the experimental data.

From our simulations of ion trajectories, we also determine the region where the channeling is concentrated, resulting in impact parameters in the range $\sim 0.5\text{--}1.44 \text{ \AA}$. This region is delimited by the straight dotted lines in Figs. 10 and 11. Large discrepancies between the theoretical models may be observed in Fig. 11 in the region of small impact parameters; however, we find no significant differences in the region explored by the present experiments. Although the theoretical curve lies between the two approaches, we find a more adequate general behavior using the Gaussian approximation.

The experimental value of the energy loss at zero exit angle for 5 keV protons was $\Delta E(0)/\Delta x = 5.8 \text{ eV/\AA}$. We note that this value agrees very well with the theoretical values of dE/dx near the center of the channel shown in Fig. 10. A similarly good agreement, with differences in the range of 5–10 %, was obtained in all the cases studied for protons and He ions.

V. MOLECULAR EFFECT

The difference between the energy-loss curves for simple proton beams and for the proton fragments produced by incident H_2^+ shown in Fig. 3, together with the difference in the characteristics of the energy-loss spectra shown in Fig. 4, indicate the possibility of a molecular or vicinage effect in the energy loss of correlated protons moving through the crystal under channeling conditions, an effect that was predicted in Ref. [23]. For the present low-energy range, this difference is expected to be negative (i.e., a reduction of the energy loss due to vicinage effects) according to previous experiments with polycrystal and monocrystal foils reported in Refs. [38,39,24], respectively; a calculation based on quantum scattering theory [40] also yields a negative vicinage effect in the low-energy range. A recent review of this subject was given in Ref. [41].

In the present experiments, we interpret this molecular effect as a result of the combination of two alternative processes: (a) protons that enter into adjacent channels and follow uncorrelated channeling trajectories, with relatively larger internuclear distances and negligible vicinage effects (we recall that vicinage effects are of short range in this low-energy regime [40]), and (b) protons that enter together in the same channel and experience a type of correlated motion, maintaining relatively close distances and being affected by the (negative) vicinage effect in the energy loss.

Following this reasoning, we aim at separating the energy-loss spectrum for proton fragments into two components, corresponding to the cases (a) and (b) mentioned above. To do this in an unambiguous way we first calculate the probability that the two protons of an incident H_2^+ molecule, having an internuclear distance r_0 and with random orientation of the internuclear axis, fall into the same channel (with a complementary fraction of protons entering into adjacent channels). The method to calculate this is described in the Appendix. Assuming an internuclear distance of about 1.3 \AA [42], the analysis yields a probability factor $P_{\text{ch}} = 0.45$ for the possibility that two such protons enter into the same channel.

Then, we perform a deconvolution of the experimental spectrum into two energy-loss curves as described in the following. The curve indicated as “total” in Fig. 12 is the original spectrum for the H^+ fragments (the same as in Fig. 4). We denote by S_{tot} the area under this curve. The two components are determined in the following way: first we plot the data curve A corresponding to the fraction of uncorrelated protons, which is a scale reproduction of the experimental spectrum resulting from proton beams (Fig. 4), but with an area scaled according to $(1 - P_{\text{ch}})S_{\text{tot}}$; and then we determine a curve B by the difference between the two previous data curves (total and A). Obviously this procedure assures that curve B has the expected area $P_{\text{ch}}S_{\text{tot}}$ and preserves the probabilities calculated for processes (a) and (b) in the Appendix. Note also that, in this way, curve B is determined by subtraction of two experimental curves.

The result of this deconvolution is represented in Fig. 12, which shows how the total spectrum separates into two components due to correlated (curve B) and uncorrelated protons (curve A). We clearly observe that curve B shows a vicinage

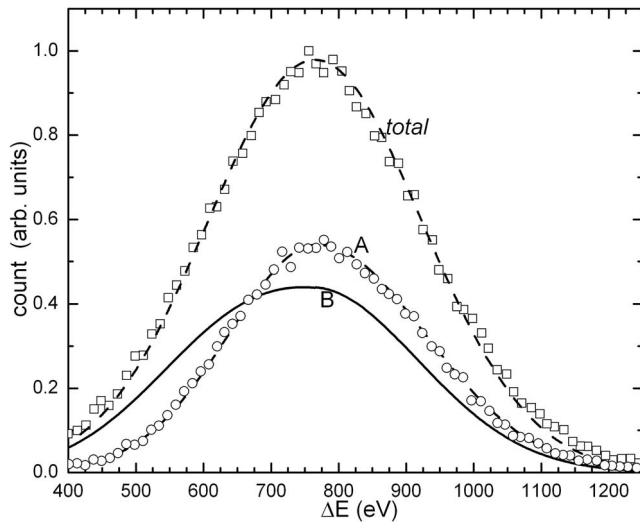


FIG. 12. Experimental energy-loss spectrum of the emerging H⁺ fragments obtained from the incidence of 5 keV/u H₂⁺ ions (curve “total”). Curve A reproduces the energy losses of 5 keV H⁺ with a scale factor as determined in the text. Curve B represents the deduced spectrum corresponding to fragments channeled within the same channel (correlated protons).

effect consisting in a displacement of the curve and hence a reduced energy loss. The magnitude of the effect, represented by the shift in the mean energy-loss values of curves A and B, is 52 ± 10 eV (which corresponds to the measured difference of about 20 eV between the experimental curves A and “total,” in correspondence also with Fig. 3). The value of the internuclear distance assumed in this case was $r_0 = 1.3$ Å [42].

A more complete analysis for different r_0 values is shown in Fig. 13, which compares the deconvolution of the energy-loss spectra of the emerging fragments (for the same case of

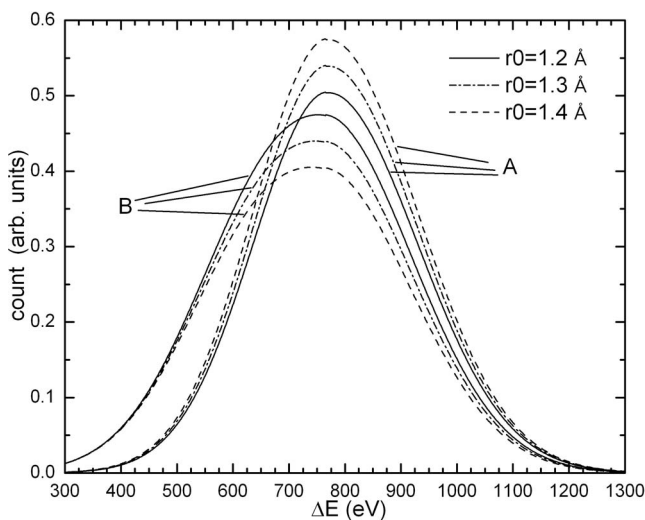


FIG. 13. Energy-loss spectra of the emerging fragments from the incidence of 5 keV/u H₂⁺ ions for different internuclear distances r_0 . Curves A and B represent the deduced spectra corresponding to the fraction of uncorrelated and correlated protons, respectively.

incidence of 5 keV/u H₂⁺ ions) for $r_0 = 1.2, 1.3,$ and 1.4 Å. The vicinage effect (energy shift) in these cases varies from 57 ± 10 to 49 ± 10 eV.

VI. SUMMARY AND CONCLUSIONS

We have studied the dependence of the energy loss on the exit angle for protons, dissociation fragments of H₂⁺, and helium ions channeled along the $\langle 100 \rangle$ direction in 120–134 Å gold crystals, at the low-velocity limit. We also investigated the energy spectra of transmitted protons produced by the dissociation of incident hydrogen molecules, which show a molecular effect for all the observed angles.

The energy loss was modeled using two alternative approaches, (i) the Oen-Robinson model, Eq. (3), and (ii) a Gaussian model, Eq. (4), containing only one fitting parameter. The comparisons provide additional information on the impact-parameter dependence of the energy loss for channeled ions in the present range of low energies. The computational simulations are in agreement with the experimental results when the energy transfer per atom to the target electrons includes a contribution of about 70% (or more) from the term that is independent of the impact parameter. The information obtained from the experimental and simulation results was compared with theoretical predictions of the stopping power versus the radial distance and the energy transfer per atom versus the impact parameter, based on local density calculations and low-energy stopping power models. By modeling the energy transfer per atom with a Gaussian dependence on the impact parameter, the calculated energy losses are in good agreement with the experimental results and show a more adequate impact-parameter dependence than in the original Oen-Robinson model. The stopping forces at the center of the channel for both protons and helium ions, calculated from the theoretical models, are ~ 5 – 10 % lower than the experimental values of energy losses measured at zero detection angle. We consider this as a fairly good agreement, taking into account the complexity of the phenomenon and the assumptions built into the theoretical free electron gas modeling.

The observed molecular effect may be explained in terms of the vicinage effect in the energy loss of those pairs of protons that enter into the same channel of the crystal, so that their interactions with the electrons are modified by interference effects. These results may be of interest for future simulations of the energy loss of correlated protons in channeling.

In summary, and with a wider view, the present study shows a direction of interest for further studies on channeling energy losses in various crystalline materials by combining basic stopping power models with standard or novel simulation codes.

ACKNOWLEDGMENTS

We are grateful to Dr. J. E. Valdés and Dr. P. Vargas for providing tabulated values of local electron densities in crystalline gold. Partial support for this work was provided by ANPCYT of Argentina (Project No. PICT R122/02). E.A.F., F.D.C., and M.L.M. acknowledge support from Consejo Na-

cional de Investigaciones Científicas y Técnicas (CONICET), Argentina.

APPENDIX

Here we analyze the fraction of proton pairs, obtained from an incident H_2^+ molecule, that may enter into the same channel after hitting the crystal surface. These pairs of protons can be affected by the vicinage effect in the energy loss, while the complementary fraction, corresponding to pairs of protons that enter into adjacent channels, are assumed to channel in an uncorrelated way, i.e., with negligible vicinage effect.

Let us first consider two protons from an incident H_2^+ molecule, hitting the crystal surface with internuclear distance r_0 and with its internuclear axis oriented with an angle θ with respect to the normal to the surface, having a projection $r_\perp = r_0 \sin \theta$ on the crystal plane. In Fig. 14 we show a transverse view of a single channel, defined by a square with sides of length $a_0/2$, and so with total area $A = a_0^2/4$, a_0 being the lattice constant. We separate this area in the following way: (i) the central region with area $A_1 = (a_0/2 - r_\perp)^2$, (ii) a set of four rectangles with total area $A_2 = 4(r_\perp/2)(a_0/2 - r_\perp)$, and (iii) the four small wedges with combined area $A_3 = (1 - \pi/4)r_\perp^2$.

Then we take as a reference the point of incidence $P_i = (x, y)$ of the geometrical center of the incident molecule on the crystal plane, and assume random orientation of the internuclear axis. It is evident that if the point P_i falls in the central region A_1 both protons will enter the same channel and will experience some type of correlated motion inside it. Next we consider the case where the point P_i falls in the region A_2 (as in Fig. 15). Then, it may be shown by simple geometrical considerations that the fraction of those pairs that will enter into the selected channel is given by

$$f(y) = \frac{2\alpha}{\pi} = \frac{2}{\pi} \arcsin\left(\frac{2y}{r_\perp}\right), \quad (A1)$$

where y is the coordinate indicated in the figure, and α is defined by the case where one of the protons hits the border

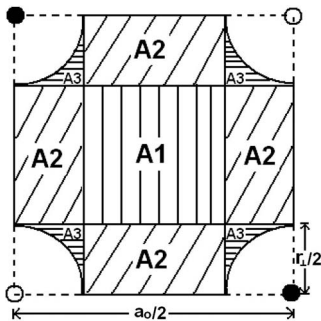


FIG. 14. Different zones where the H_2^+ molecule can impact the crystal surface. If the molecule impacts in the area A_1 then the two proton fragments will enter in the same channel. In the regions A_2 and A_3 the probability for the process is given by the factors f_m and g_m calculated in the text. The lattice parameter of gold is denoted by a_0 and $r_\perp = r_0 \sin \theta$, where r_0 is the internuclear distance of H_2^+ .

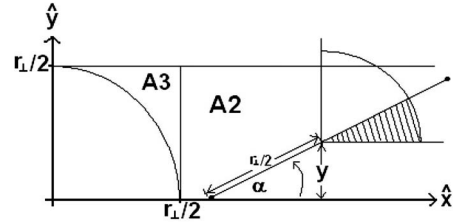


FIG. 15. Illustration of the case when the molecule hits the crystal surface in region A_2 and its geometrical center is at ordinate y .

of the channel. Hence, the mean value f_m (probability factor) for this kind of event is given by

$$f_m = \frac{2}{r_\perp} \int_0^{r_\perp/2} \frac{2}{\pi} \arcsin\left(\frac{2y}{r_\perp}\right) dy, \quad (A2)$$

which yields a numerical value $f_m = 0.363$ (independent of r_\perp). Going one step further, when the point of incidence $P_i = (x, y)$ falls in one of the regions denoted A_3 (Fig. 16) the probability factor becomes

$$g(x, y) = 1 - \frac{2}{\pi}(\beta + \gamma) = 1 - \frac{2}{\pi} \left[\arccos\left(\frac{2y}{r_\perp}\right) + \arccos\left(\frac{2x}{r_\perp}\right) \right] \quad (A3)$$

and its average is

$$g_m = \frac{\int_0^{r_\perp/2} \int_0^{r_\perp/2} \frac{g(x, y)}{\sqrt{(r_\perp/2)^2 - x^2}} dy dx}{\int_0^{r_\perp/2} \int_0^{r_\perp/2} \frac{1}{\sqrt{(r_\perp/2)^2 - x^2}} dy dx} \quad (A4)$$

which yields $g_m = 0.210$ (independent of r_\perp).

Summing up, we assign probability factors 1, f_m , and g_m to the corresponding areas A_1 , A_2 , and A_3 , and we calculate the probability that a pair of protons with internuclear projection r_\perp will lead to two correlated protons entering the same channel as

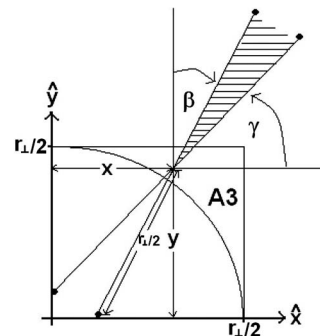


FIG. 16. Illustration of the case when the molecule hits the crystal surface in region A_3 with its center located at (x, y) .

$$P(r_{\perp}) = \frac{A_1(r_{\perp}) + f_m A_2(r_{\perp}) + g_m A_3(r_{\perp})}{(a_0/2)^2}. \quad (\text{A5})$$

Finally, we must take into account the probability of obtaining incident molecules with angular orientation θ (and so with $r_{\perp} = r_0 \sin \theta$) from a beam with random orientations, namely,

$$\frac{2\pi \sin \theta d\theta}{4\pi} = \frac{1}{2} \sin \theta d\theta, \quad (\text{A6})$$

and then we finally obtain the combined probability for correlated channeling of protons corresponding to random incident molecules as

$$P_{\text{ch}} = \frac{1}{2} \int_0^{\pi} P(r_0 \sin \theta) \sin \theta d\theta. \quad (\text{A7})$$

In the present case of the $\langle 100 \rangle$ channel of Au, where $a_0 = 4.078 \text{ \AA}$, and assuming $r_0 = 1.3 \text{ \AA}$, we obtain the numerical result $P_{\text{ch}} = 0.449$.

-
- [1] M. Robinson and O. Oen, Phys. Rev. **132**, 2385 (1963).
 [2] C. Andreen and R. Hines, Phys. Rev. **151**, 341 (1966); **159**, 285 (1967).
 [3] D. Gemmell and R. Holland, Phys. Rev. Lett. **14**, 945 (1965).
 [4] R. Holland and D. Gemmell, Phys. Rev. **173**, 344 (1968).
 [5] W. Gibson, C. Erginsoy, H. Wegner, and B. Appleton, Phys. Rev. Lett. **15**, 357 (1965).
 [6] J. Lindhard, Mat. Fys. Medd. K. Dan. Vidensk. Selsk. **34** (14) (1965).
 [7] C. Cohen and D. Dauvergne, Nucl. Instrum. Methods Phys. Res. B **225**, 40 (2004).
 [8] R. Ishiwari, N. Shiomi, T. Katayama-Kinoshita, and F. Sawada-Yasue, J. Phys. Soc. Jpn. **29**, 577 (1975).
 [9] P. Apel and U. Müller-Jahreis, Phys. Status Solidi A **33**, K129 (1976).
 [10] R. Blume, W. Eckstein, and H. Verbeek, Nucl. Instrum. Methods **168**, 57 (1980).
 [11] R. Ishiwari, N. Shiomi, and N. Sakamoto, Phys. Rev. A **25**, 2524 (1982).
 [12] M. Jakas, G. Lantschner, J. Eckardt, and V. Ponce, Phys. Rev. A **29**, 1838 (1984).
 [13] G. H. Lantschner, J. C. Eckardt, M. M. Jakas, N. E. Capuj, and H. Ascolani, Phys. Rev. A **36**, 4667 (1987).
 [14] N. Kabachnik, Nucl. Instrum. Methods Phys. Res. B **69**, 76 (1992).
 [15] A. Bendyakov *et al.*, Nucl. Instrum. Methods Phys. Res. B **115**, 168 (1996).
 [16] Yueyuan Xia, Chunyu Tan, and W. Lennard, Nucl. Instrum. Methods Phys. Res. B **90**, 41 (1994).
 [17] S. Gelfort *et al.*, Nucl. Instrum. Methods Phys. Res. B **115**, 315 (1996).
 [18] W. Arnoldbik, V. Khodyrev, G. Iferov, and D. Boerma, Nucl. Instrum. Methods Phys. Res. B **136-138**, 91 (1998).
 [19] M. Famá, G. Lantschner, J. Eckardt, C. Denton, and N. Arista, Nucl. Instrum. Methods Phys. Res. B **164**, 241 (2000).
 [20] M. Famá, J. C. Eckardt, G. H. Lantschner, and N. R. Arista, Phys. Rev. A **62**, 062901 (2000).
 [21] G. Högberg, H. Nordén, and R. Skoog, Phys. Status Solidi **42**, 441 (1970).
 [22] R. Blume, W. Eckstein, H. Verbeek, and K. Reichelt, Nucl. Instrum. Methods Phys. Res. **194**, 67 (1982).
 [23] N. R. Arista and V. H. Ponce, J. Phys. C **8**, L188 (1975).
 [24] J. E. Valdés, C. Parra, J. Díaz-Valdés, C. D. Denton, C. Agurto, F. Ortega, N. R. Arista, and P. Vargas, Phys. Rev. A **68**, 064901 (2003).
 [25] M. Robinson, computer code, Version 15, MARLOWE.
 [26] D. O'Connor and J. Biersack, Nucl. Instrum. Methods Phys. Res. B **15**, 14-19 (1986).
 [27] O. Oen and M. Robinson, Nucl. Instrum. Methods **132**, 647 (1976).
 [28] M. J. Puska and R. M. Nieminen, Phys. Rev. B **27**, 6121 (1983).
 [29] P. Vargas, J. E. Valdés, and N. R. Arista, Phys. Rev. A **53**, 1638 (1996).
 [30] J. E. Valdés and P. Vargas (private communication).
 [31] A. F. Lifschitz and N. R. Arista, Phys. Rev. A **57**, 200 (1998).
 [32] P. M. Echenique and M. E. Uranga, in *Interaction of Charged Particles with Solids and Surfaces*, edited by A. Grass Marti, H. M. Urbassek, N. R. Arista, and F. F. Flores, NATO Advanced Studies Institute, Series B: Physics (Plenum, New York, 1991), Vol. 271.
 [33] J. Ziegler, J. Biersack, and U. Littmark, *The Stopping and Range of Ions in Solids* (Pergamon Press, Oxford, 1985), Vol. 1.
 [34] T. L. Ferrell and R. H. Ritchie, Phys. Rev. B **16**, 115 (1977).
 [35] P. Sigmund, Phys. Rev. A **26**, 2497 (1982).
 [36] E. Bonderup, Mat. Fys. Medd. K. Dan. Vidensk. Selsk. **35**, No. 17, 1 (1967); E. Bonderup and P. Hvelplund, Phys. Rev. A **4**, 562 (1971).
 [37] E. Fermi and E. Teller, Phys. Rev. **72**, 399 (1947).
 [38] J. C. Eckardt, G. H. Lantschner, N. R. Arista, and R. A. Baragiola, J. Phys. C **11**, L851 (1978).
 [39] R. Levi-Setti, K. Lam, and T. R. Fox, Nucl. Instrum. Methods Phys. Res. **194**, 281 (1982).
 [40] R. Diez Muiño and A. Salin, Phys. Rev. B **62**, 5207 (2000).
 [41] N. R. Arista, Nucl. Instrum. Methods Phys. Res. B **164-165**, 108 (2000).
 [42] W. Brandt, A. Ratkowski, and R. H. Ritchie, Phys. Rev. Lett. **33**, 1325 (1974).